

# Optimal modeling of antenna beam

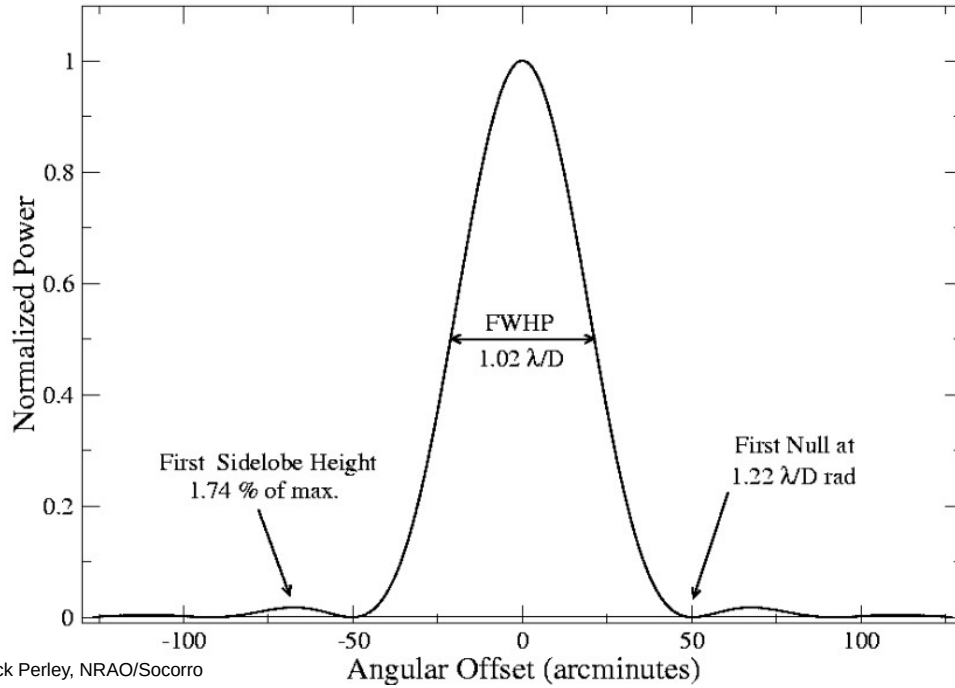
Morteza Pashapour-Ahmadabadi

# Radio Antenna Beam

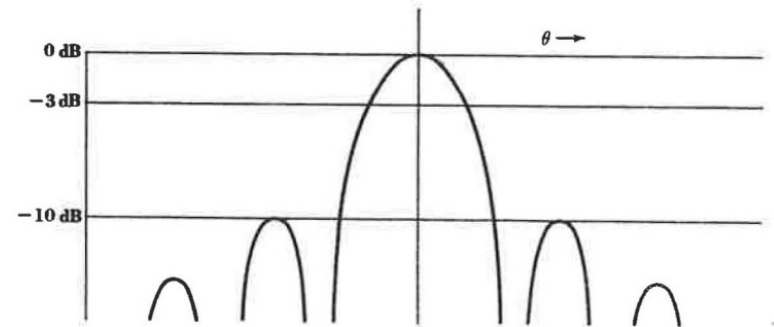
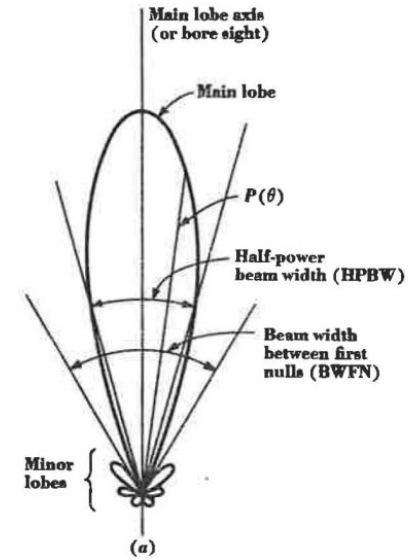
- If the pattern is measured at a sufficient distance from the antenna so that an increase in the distance causes no change in the pattern, the pattern is the far-field pattern:  $r > 2D^2/\lambda$

Antenna Power Response at 1 GHz

25-meter diameter, uniform illumination



Rick Perley, NRAO/Socorro



Kraus, J., 1982

$$r_1 = 0.62 \sqrt{\frac{D^3}{\lambda}}$$

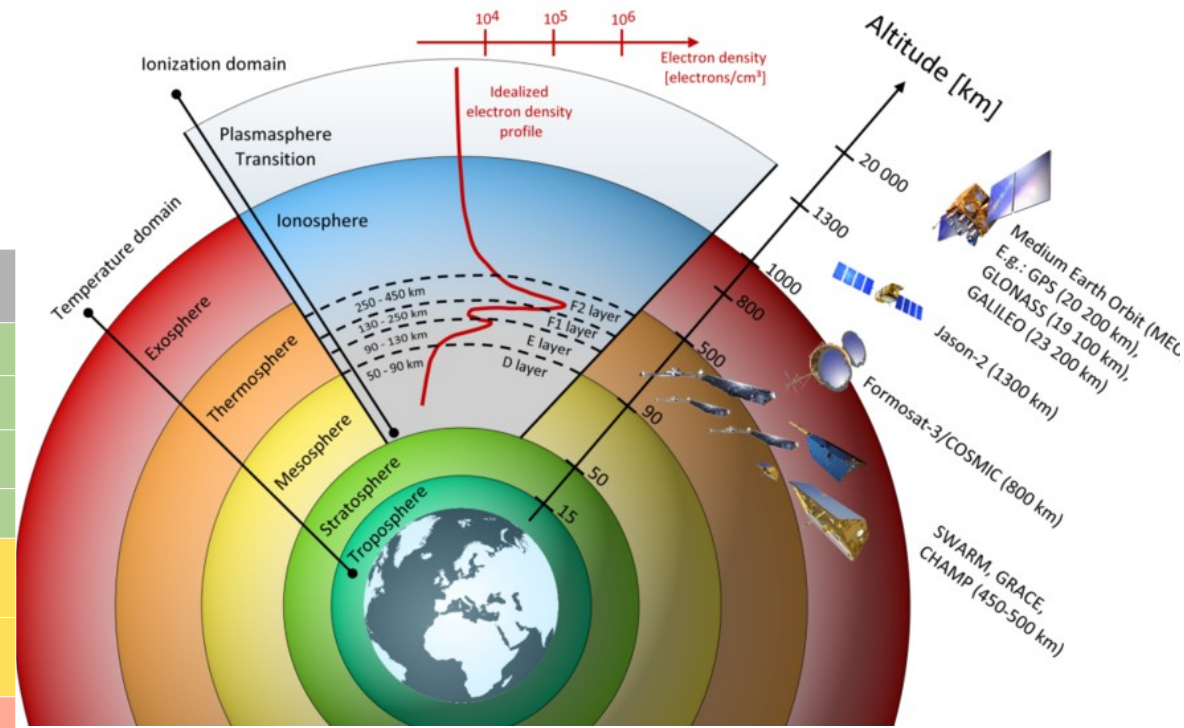
$r < r_1$  reactive near field

$$r_2 = \frac{2D^2}{\lambda}$$

$r_1 < r < r_2$  radiating near field

$r > r_2$  far field

Antenna	Size (m)	Frequencies (GHz)	Wavelength (cm)	Far field (km)
SKA MPI	15	UHF: 0.5 - 1	60 - 30	0.75 - 1.5
		L: 1 - 2	30 - 15	1.5 - 3
		S: 2 - 4	15 - 7.5	3 - 6
		Ku: 12 - 14	2.5 - 1.7	18-26
Meerkat	13.5	L: 1 - 2	30 - 15	1.2 - 2.5
		S: 2 - 4	15 - 7.5	2.5 - 5
LBA station	60	0.054	550	1.3
HBA <sub>core</sub>	30	0.15	200	0.9
HBA <sub>remote</sub>	40	0.15	200	1.6
HBA <sub>international</sub>	60	0.15	200	3.6



Florian Seitz, Deutsches Geodätisches Forschungsinstitut, TUM

Low Earth Orbit (LEO) 160 to 2000 km

Medium Earth Orbit (MEO) 2000 to 35000 km

Geosynchronous Orbit (GEO) approx. 36000 km

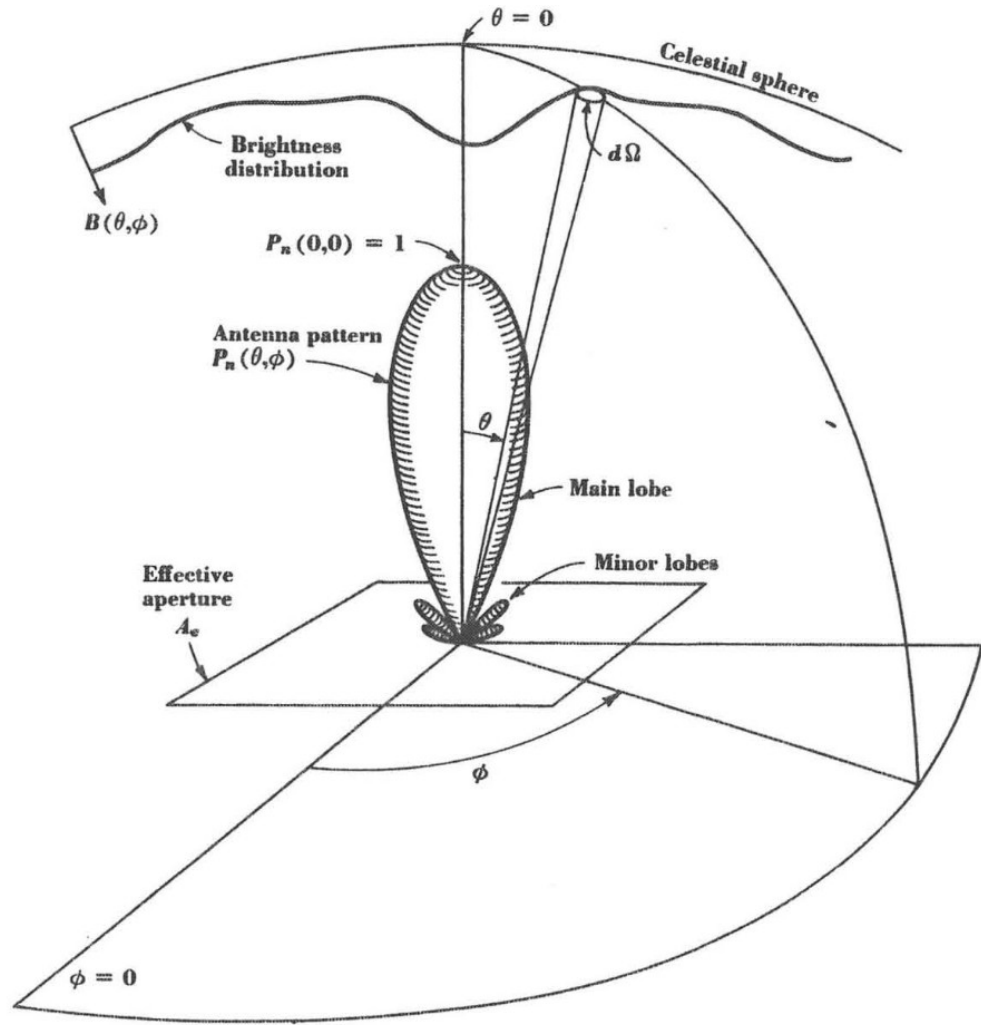
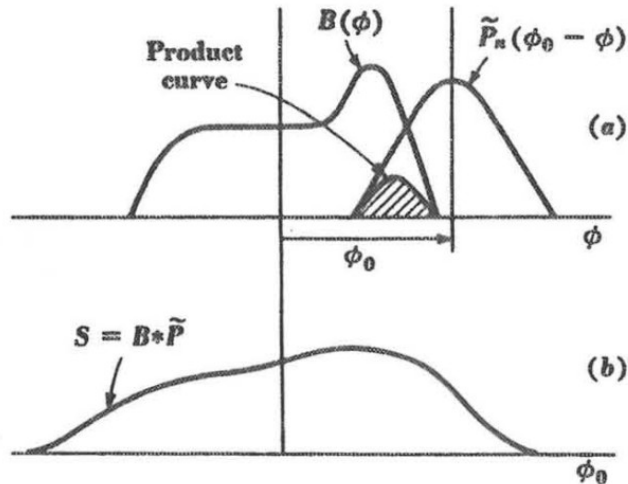
The antenna pattern  $P_n(\theta, \phi)$  is like a weighting function

$$S = \iint_{\text{source}} B(\theta, \phi) P_n(\theta, \phi) d\Omega$$

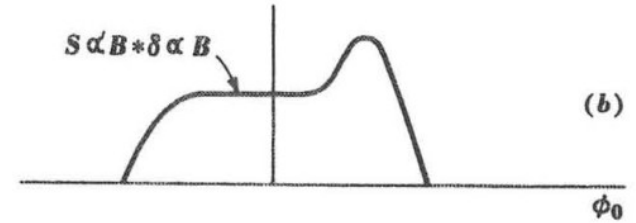
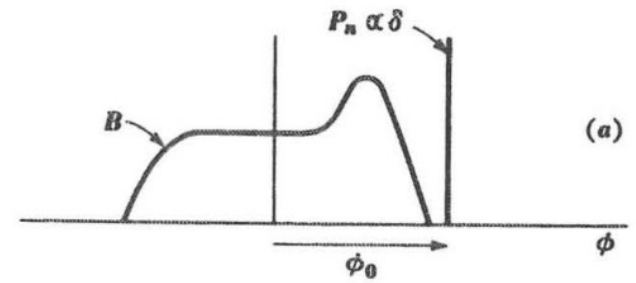
- (a) The true brightness distribution  $B$  scanned by, or convolved with, the antenna pattern  $P$ .  
 (b) The observed flux-density distribution  $S$ .

$$S(\phi_0) = \int B(\phi_0 - \phi) \tilde{P}_n(\phi) d\phi$$

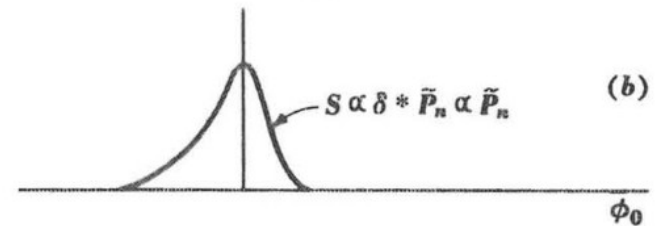
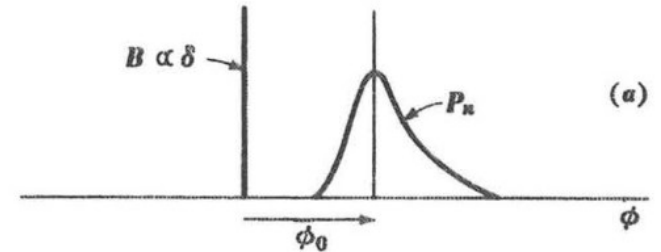
$$S = B * \tilde{P}$$



- For an infinitely sharp antenna pattern (perfect observing instrument) the observed distribution is identical with the true distribution.



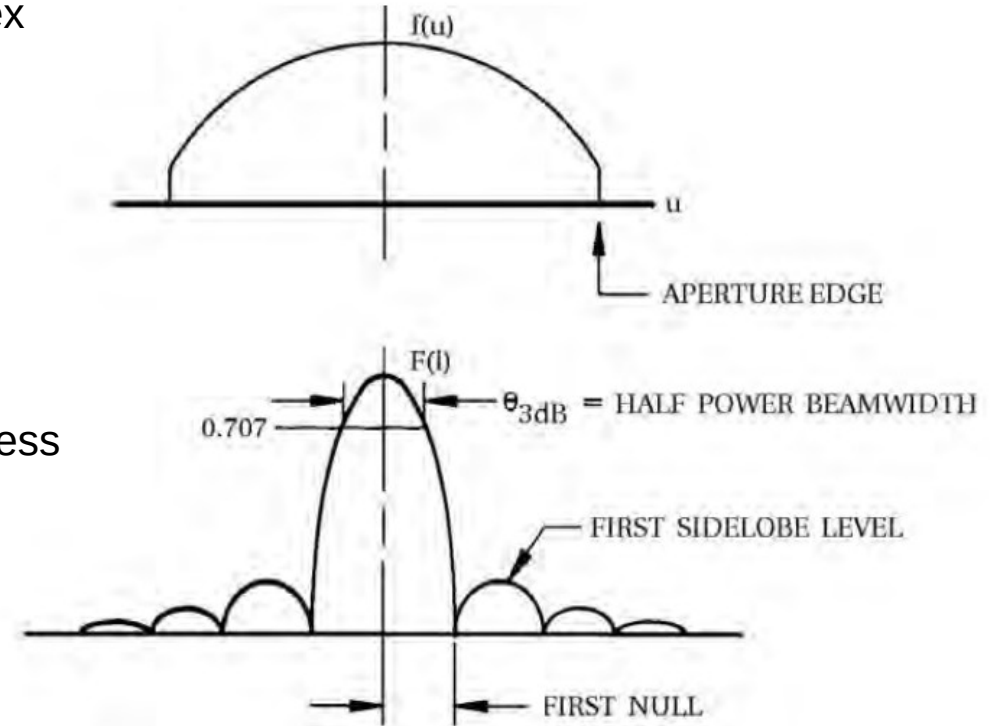
- For a point source, the observed distribution is the same as the mirror image of the antenna pattern.



- Relationship between the complex voltage distribution of the field in the aperture of an antenna and the complex far-field voltage radiation pattern.

$$f(u, v) = \iint_{-\infty}^{\infty} F(l, m) e^{-2\pi i(vl + um)} dl dm$$

- It is analogous to the one between the source brightness distribution and its visibility function.



## (1)

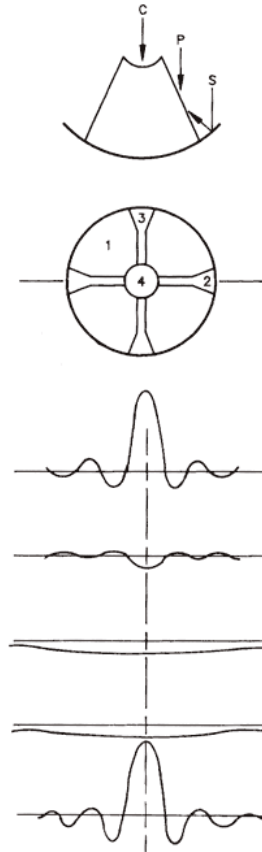
- Taking the uniform distribution as reference, the more tapered distributions (triangular and cosine) have larger beam widths but smaller minor lobes, while the most gradually tapered distributions (cosine squared and Gaussian) have still larger beam widths but no minor lobes.
- An inverse taper (less amplitude at the center than at the edge), as shown in (f), yields a smaller beam width but larger minor lobes than for the uniform distribution.
- Such an inverse taper might inadvertently result from aperture blocking due to a feed structure in front of the aperture.

## (2)

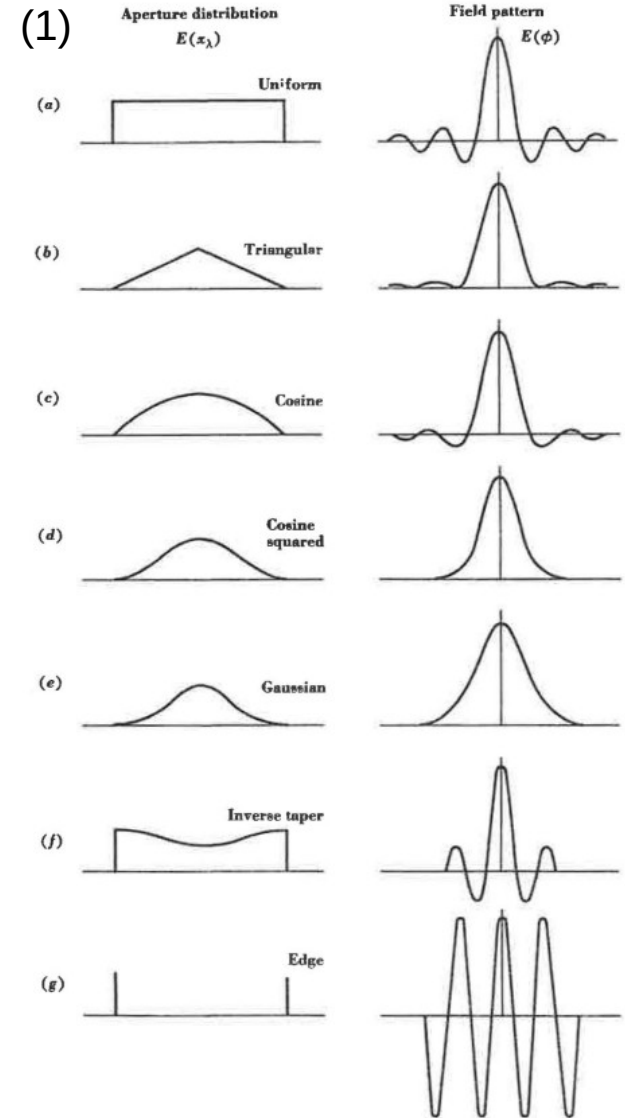
- If we do the Fourier Transform of each part of the regions 1, 2, 3 and 4 in (b) :

(c) is the FT of the unblocked aperture,  
(d) is the FT of part 2 (shown negative because it is a blockage),  
(e) is the FT of part 3, also negative,  
(f) is the FT of part 4,  
(g) is the sum of the FT's.

## (2)



## (1)

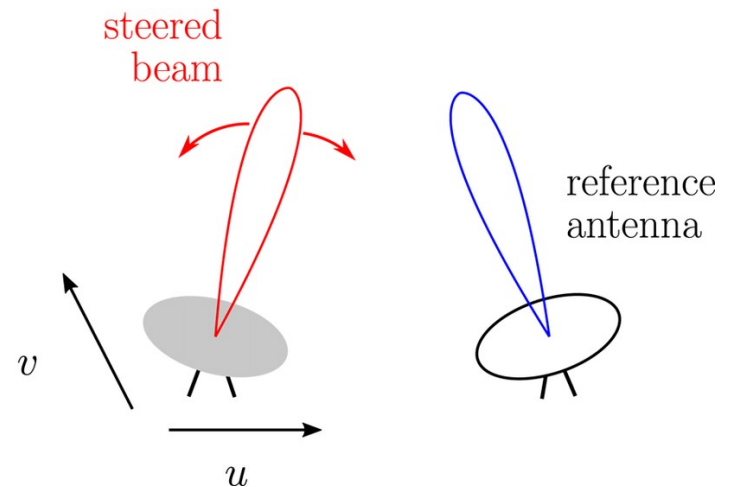
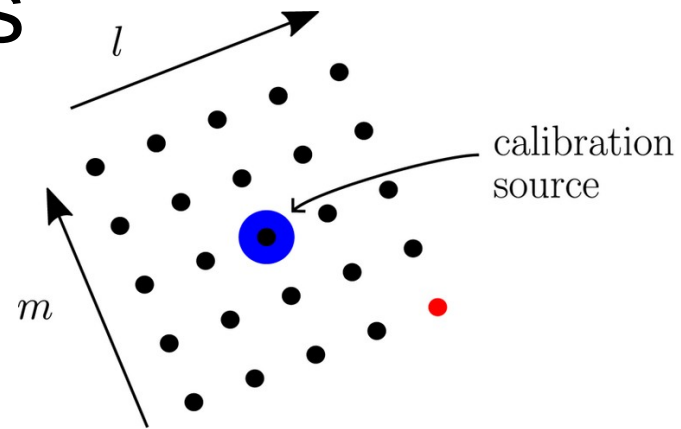


# Primary beam measurements

- **Electromagnetic simulations** (theoretical PB models) like CST or FEKO
- **PB holography**
  - using astronomical sources (the sun, the moon and known bright radio sources such as Cassiopeia A, Taurus A, Cygnus A, and Virgo A): the number of sources is limited and decreases for smaller radio dishes, the fluxes and the sizes of these sources can fluctuate over time!
  - using satellites (Geosynchronous, GPS, ...): limited frequencies, high polarized signal, but fairly high and regular intensity!
  - using Drones
  - Using earth-bound transmitter: a distance of several hundreds of meters to a few kilometers and be at an elevation angle of less than 10 degree, mostly in the near-field of an antenna.

# Holographic measurements

- While one antenna (reference antenna) tracks the target, the other antenna (moving antenna) executes a raster pattern (on the fly mapping) about the target position.
- With dish antennas are sophisticated because the antennas have to be adjusted mechanically and the calibration source changes its celestial position during the process.
- Using Geosynchronous satellites to remove the time-varying time arrival between two antennas.



## VLA L-band beam using holography:

- The variation of the FWHM of the average holographic primary lobe decreases, at first order, as a function of  $1/\nu$ .
- The other effect is related to the presence of a standing wave between the primary and secondary reflector of the antenna. It induces a strong frequency ripple on the whole beam Pattern.
- The third effect is the possible attenuation of the ripple amplitude as the frequency increases.

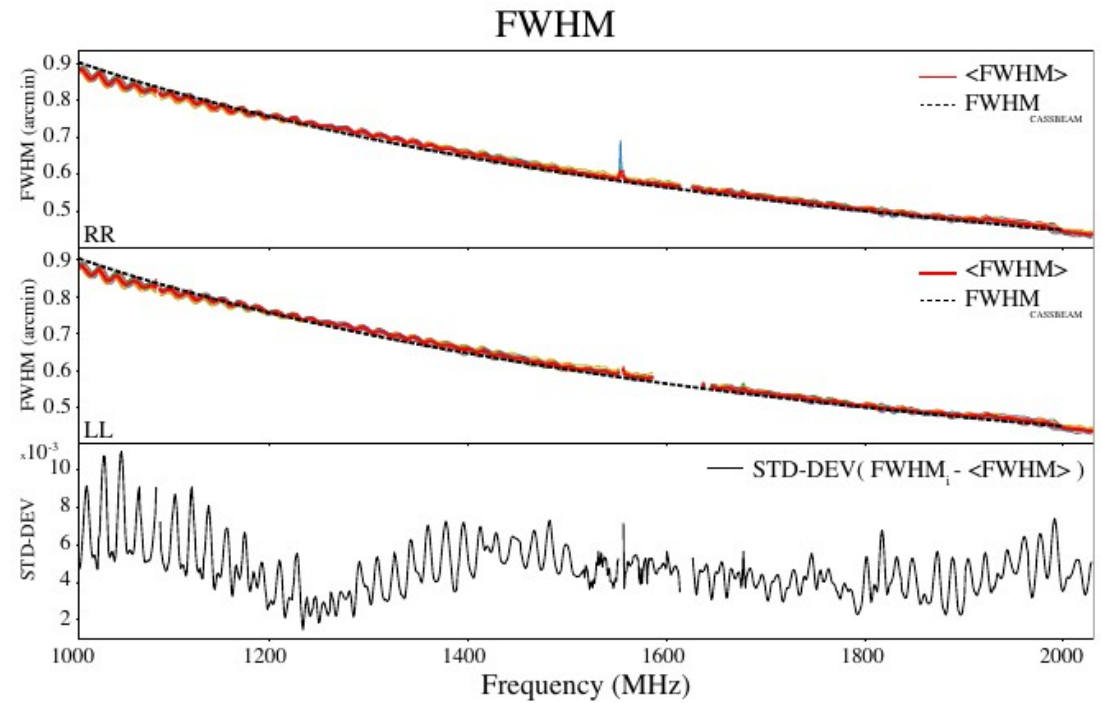


**Figure 3.** Evolution of the fitted FWHM as a function of frequency for the *RR* and *LL* beam amplitude. The average FWHM variation is plotted with the red line. The dash line represent the FWHM derived from the fit of the *Cassbeam* model. (Bottom row) Standard deviation across the 12 antennas after removing the average trend.

# Sources of variations

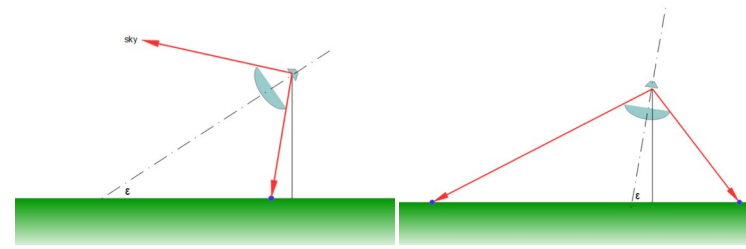
The measurements are generally done in some given situations but each combination of following uncertainties changes the beam:

## Frequency-dependent variations:

- Standing waves
- Blockage of the arms
- FWHM of the beam
- Orthomode transducer

## Continuous variations:

- Gravitational loading for dish antennas (elevation dependent)
- Dish surface deformation (loading, temperature, ... dependent)
- Spillover noise (elevation dependent)
- Atmosphere effects (wind, temperature, ... dependent)
- Earth soil effect (on ground plane antenna: elevation dependent)
- Feed arm changes for off-axis Gregorian antennas (loading, temperature dependent )
- Ionosphere effects (activity of sun,... dependent)



Elevation Scan of the Sky Measures Antenna Spill-Over, Joachim Köppen  
Kiel, 2021

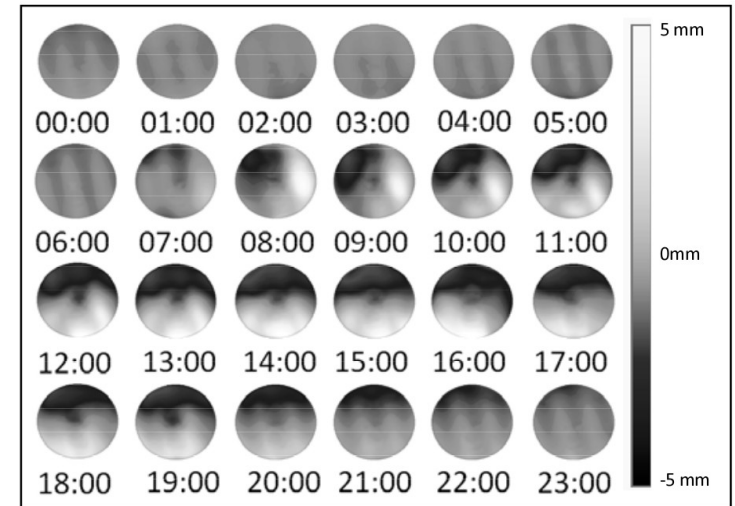
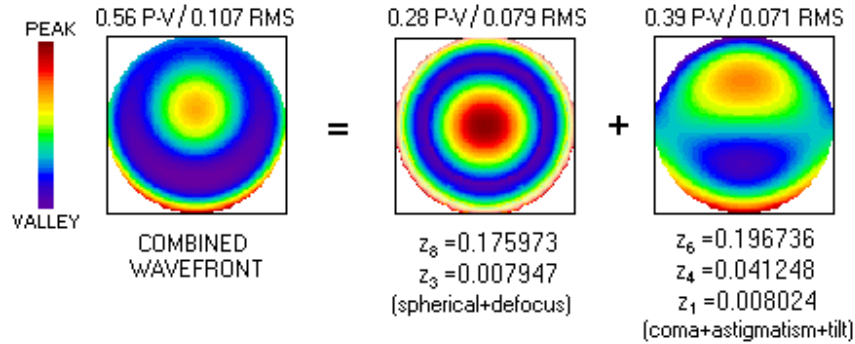


Figure 19: Grayscale display of deformation of one dish (as determined from holography) during a 24-hour period in August, 2008. Evidence of sunrise appears at ~08:00, and the deformations maximize at 13:00 hours (daylight savings time) and then decay after sunset after 19:00 hours. The dish was facing 13° east of south, hence the sunrise / sunset patterns are not symmetrical.

After measurement, the people take use of different types of beam pattern modeling based on basis functions:

- Gaussian and Airy disk fitting model
- Zernike polynomials
- Characteristic Basis Function Patterns (CBFP)

An expanded set of Zernike polynomials includes any chosen number of higher-order terms, in addition to the lower-order terms and they are often given in the form of a simple  $Z_i$ , with the subscript 'i' indicating term's ordering number, and referred to as Zernike coefficients



Sacek, V., 2006

1	2	3	4	5			6				
				#	ZERNIKE TERM (often erroneously referred to as coefficient)	ZERNIKE ORTHOGONAL CIRCLE POLYNOMIAL		RMS ERROR (Zernike coefficient's absolute value)	ABERRATION		WF Map <sup>[2]</sup> w/ANSI sign PEAK VALLEY
									Name	Standard aberration function <sup>[1]</sup>	
					Paraxial focus						
0	$Z_0$	1	$Z_0$	PISTON	-	-	$Z_0^0$				
1	$Z_1$	$\rho \cos\theta$	$Z_1 / 2$	DISTORTION/TILT	$\rho \cos\theta$	$\rho \cos\theta$	$Z_1^{-1}$				
2	$Z_2$	$\rho \sin\theta$	$Z_2 / 2$		-	-					
3	$Z_3$	$2\rho^2-1$	$Z_3 / \sqrt{3}$	DEFOCUS/FIELD CURVATURE	$\rho^2$	$\rho^2$ $\rho^2-0.5*$	$Z_2^0$				
4	$Z_4$	$\rho^2 \cos 2\theta$	$Z_4 / \sqrt{6}$	PRIMARY ASTIGMATISM	$\rho^2 \cos^2\theta$	$\rho^2(\cos^2\theta-0.5) *$	$Z_2^2$				
5	$Z_5$	$\rho^2 \sin 2\theta$	$Z_5 / \sqrt{6}$		-	-					
6	$Z_6$	$(3\rho^3-2\rho)\cos\theta$	$Z_6 / \sqrt{8}$	PRIMARY COMA	$\rho^3 \cos\theta *$	$(\rho^3-2\rho/3)\cos\theta *$	$Z_3^{-1}$				
7	$Z_7$	$(3\rho^3-2\rho)\sin\theta$	$Z_7 / \sqrt{8}$		-	-					
8	$Z_8$	$6\rho^4-6\rho^2+1$	$Z_8 / \sqrt{5}$	BALANCED PRIMARY SPHERICAL ABERRATION	$\rho^4$	$\rho^4-\rho^2$ $\rho^4-\rho^2+1/6 *$	$Z_4^0$				
9	$Z_9$	$\rho^3 \cos 3\theta$	$Z_9 / \sqrt{8}$	ELLIPTICAL COMA (ARROWS, TREFOIL)	$\rho^3 \cos^3\theta *$	$\rho^3 \cos^3\theta *$	$Z_3^{-3}$				
10	$Z_{10}$	$\rho^3 \sin 3\theta$	$Z_{10} / \sqrt{8}$		-	-					
11	$Z_{11}$	$(4\rho^4-3\rho^2)\cos 2\theta$	$Z_{11} / \sqrt{10}$	SECONDARY ASTIGMATISM	$\rho^4 \cos^2\theta$	$(\rho^4-0.75\rho^2)\cos^2\theta *$	$Z_4^2$				
12	$Z_{12}$	$(4\rho^4-3\rho^2)\sin 2\theta$	$Z_{12} / \sqrt{10}$		-	-					
13	$Z_{13}$	$(10\rho^5-12\rho^3+3\rho)\cos\theta$	$Z_{13} / \sqrt{12}$	SECONDARY COMA	$\rho^5 \cos\theta$	$(\rho^5-1.2\rho^3+0.3\rho)\cos\theta *$	$Z_5^{-1}$				
14	$Z_{14}$	$(10\rho^5-12\rho^3+3\rho)\sin\theta$	$Z_{14} / \sqrt{12}$		-	-					
15	$Z_{15}$	$20\rho^6-30\rho^4+12\rho^2-1$	$Z_{15} / \sqrt{7}$	SECONDARY SPHERICAL ABERRATION	$\rho^6$	$\rho^6-1.5\rho^4+0.6\rho^2$ $\rho^6-1.5\rho^4+0.6\rho^2-0.05 *$	$Z_6^0$				

- The CBFP method uses a weighted sum of numerically defined (through simulation or measurements) orthogonal basis functions to approximate the actual radiation pattern.
- Interpolation of the weights over frequency allows accurate wideband models of the radiation pattern of interest to be generated with minimal computational and storage cost.

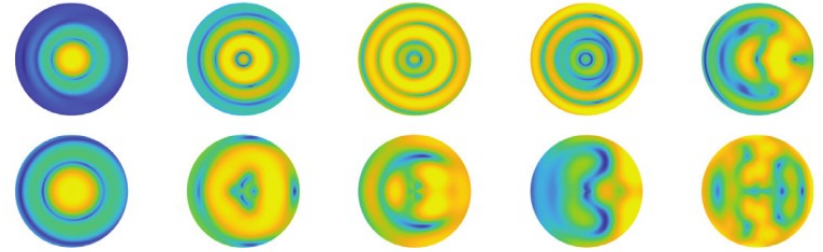


Fig. 4. Magnitude (in dB scale) of the first five CBFP modal distributions (left to right) of the phase normalized only (top) and the phase and beamwidth normalized (bottom) fields.

De Villiers, D. 2018

# Purposes of the beam modeling in this project

- To develop a telescope-independent set of methods that capture the spatial and spectral morphology of the beam in the most generic way.
- To provide a model with the smallest number of degrees of freedom, in order to only capture the relevant components of the beam and its variations.
- Once the beam is accurately represented, it can be turned into a parametric model (Jones) matrix of known structure that can be solved for during the calibration phase.

# References

- Kraus, J., 1982, "Radio Astronomy", second edition, New York: McGraw-Hill, 1966.
- De Villiers, D. 2018, "Characteristic Basis Function Pattern Modeling of Wideband Reflector Antenna Beam Pattern Frequency Variations"
- Sacek, V., 2006, "Notes on AMATEUR TELESCOPE OPTICS"  
[https://www.telescope-optics.net/zernike\\_expansion\\_schemes.htm](https://www.telescope-optics.net/zernike_expansion_schemes.htm)
- Harp et al, 2009, "Primary Beam and Dish Surface Characterization at the Allen Telescope Array by Radio Holography"
- Taylor, G. B.; Carilli, C. L.; Perley, R. A., Synthesis Imaging in Radio Astronomy II, A Collection of Lectures from the Sixth NRAO/NMIMT Synthesis Imaging Summer School. ASP Conference Series, Vol. 180, 1999